Published in "Proceedings of the National Academy of Sciences 115 (4): E705–E714, 2018"
which should be cited to refer to this work.

Impaired lymphoid extracellular matrix impedes antibacterial immunity in epidermolysis bullosa

Alexander Nyström[a,1], Olivier Bornert[a], Tobias Kühl[a], Christine Gretzmeier[a], Kerstin Thriene[a], Jörn Dengjel[a,b], Andrea Pfister-Wartha[a], Dimitra Kiritsi[a], and Leena Bruckner-Tuderman[a]

[a]Department of Dermatology, Faculty of Medicine, Medical Center – University of Freiburg, University of Freiburg, 79104 Freiburg, Germany; and [b]Department of Biology, University of Fribourg, 1700 Fribourg, Switzerland

Genetic loss of collagen VII causes recessive dystrophic epidermolysis bullosa (RDEB), a skin fragility disorder that, unexpectedly, manifests also with elevated colonization of commensal bacteria and frequent wound infections. Here, we describe an unprecedented systemic function of collagen VII as a member of a unique innate immune-supporting multiprotein complex in spleen and lymph nodes. In this complex, collagen VII specifically binds and sequesters the innate immune activator cochlin in the lumen of lymphoid conduits. In genetic mouse models, loss of collagen VII increased bacterial colonization by diminishing levels of circulating cochlin LCCL domain. Intraperitoneal injection of collagen VII, which restored cochlin in the spleen, but not in the skin, reactivated peripheral innate immune cells via cochlin and reduced bacterial skin colonization. Systemic administration of the cochlin LCCL domain was alone sufficient to diminish bacterial supercolonization of RDEB mouse skin. Human validation demonstrated that RDEB patients displayed lower levels of systemic cochlin LCCL domain with subsequently impaired macrophage response in infected wounds. This study identifies an intrinsic innate immune dysfunction in RDEB and uncovers a unique role of the lymphoid extracellular matrix in systemic defense against bacteria.

collagen VII | innate immunity | bacteria | recessive dystrophic epidermolysis bullosa | cochlin

Recessive dystrophic epidermolysis bullosa (RDEB) is a skin fragility disorder caused by mutations in the *COL7A1* gene encoding collagen VII, a large extracellular matrix (ECM) protein and the main component of anchoring fibrils, which ensure skin integrity (1). Mechanically induced skin blistering, painful wounds, and healing with scarring severely impede the quality of life of the affected individuals (2, 3). Injury-derived progressive soft tissue fibrosis drives formation of aggressive squamous cell carcinoma, which is the main cause of death in severe RDEB (4, 5). Collagen VII has been viewed as a rather skin-specialized protein, but extracutaneous expression also occurs (6). So far, the function of collagen VII in extracutaneous structures remains elusive. One intriguing feature of RDEB is the association with elevated colonization rates in skin and nasal cavities of commensal bacteria (3, 7). The increased bacterial burden is suggested to contribute to the patients' high predisposition to chronic infections and squamous cell carcinoma development (8–10). Although open wounds may be one factor that promotes bacterial colonization, severely affected RDEB patients show intriguingly elevated colonization with commensal pathogens compared with other individuals with large wounded areas (7, 11). These observations suggest that not the wounds per se but rather loss of collagen VII leads to dysregulation of antibacterial immunity.

With the present understanding of regulation of antibacterial defense, the connection between loss of collagen VII and increased susceptibility to bacterial colonization is challenging to make. Although cues from the ECM determine functions in many organs, its role in immunity is less well understood. Evidence is emerging that the ECM in lymphoid organs, in addition to its obvious scaffold functions (12–15), can also directly instruct mature immune cells (16). In this context, cochlin—an ECM protein with expression restricted to cochlea, lymph nodes, and spleen (16)—is of high interest. Mutations in the cochlin gene, *COCH*, result in the deafness, autosomal dominant 9 (DFNA9) syndrome, which is a syndrome with adult onset that manifests in progressive hearing loss and vestibular dysfunction (17). The physiological function of cochlin still needs elucidation, but cochlin has been suggested to be involved in mechanosensing, as well as being a local and systemic regulator of antibacterial immunity (16, 18, 19). Cochlin-deficient mice show impaired abilities to clear experimentally induced lung infection with *Pseudomonas aeruginosa* and *Staphylococcus aureus* (16).

In lymph nodes and spleen, cochlin is sequestered in lymphoid conduits (16), tube-like ECM structures composed of a collagen core surrounded by a microfibril layer and a basement membrane (20, 21). The molecular composition of conduits varies between the distinct areas of the splenic white pulp (15, 20–22), pointing to differentiated roles of individual ECM components in regulating specific immune reactions (15). In response to bacterial infection, aggrecanase-mediated processing of cochlin, sequestered in the lumen of follicular conduits, leads to systemic increase of the cochlin LCCL domain. This, in turn, activates macrophages and neutrophils peripherally and thereby stimulates bacterial clearance at infection sites (16). The mechanism of this activation is currently not completely understood, So far, no human disease has been attributed to this line of immune

Significance

We describe a unique role for the lymphoid extracellular matrix in maintaining systemic innate immunity. Our findings are based on studies of the genetic skin disorder recessive dystrophic epidermolysis bullosa in which affected individuals display dramatically increased bacterial colonization of skin and mucosa. We show that the increased colonization is a consequence of loss of the protein at fault—collagen VII—from the lymphoid extracellular matrix. Our study describes an intrinsic innate immune defect resulting from a genetic connective tissue disease. Hence, the data will have broad implications for deciphering the hitherto-underestimated regulatory role of the extracellular matrix in lymphoid organs and for the understanding of pathomechanisms in disorders of the extracellular matrix.

Author contributions: A.N. and L.B.-T. conceived the study; A.N. coordinated the study; A.N., J.D., D.K., and L.B.-T. designed research; A.N., O.B., T.K., C.G., K.T., and D.K. performed research; D.K. provided patient material and performed bacterial colonization studies of patients; A.P.-W. contributed new reagents/analytic tools; A.N., O.B., T.K., C.G., K.T., J.D., A.P.-W., D.K., and L.B.-T. analyzed data; A.P.-W. provided analyses of bacteria; and A.N. and L.B.-T. wrote the paper.

The authors declare no conflict of interest.

[1]To whom correspondence should be addressed. Email: alexander.nystroem@uniklinik-freiburg.de.

http://doc.rero.ch

regulation, presumably because known mutations in the *COCH* gene are rare and genotype–phenotype correlations have not been extensively investigated (16, 17).

Based on the observation that RDEB is associated with drastically elevated susceptibility to bacterial colonization of skin, we addressed the possible involvement of collagen VII in antibacterial defense mechanisms. Our study revealed that extracutaneous collagen VII present in lymphoid conduits supports systemic innate immune reactions. In the conduits, collagen VII is a direct interaction partner of cochlin and a component of a multiprotein complex that establishes correct cochlin presentation. Loss of collagen VII in mice evoked concurrent loss of cochlin from lymphoid conduits, resulting in an inability to activate innate immune cells in skin and subsequent increase in bacterial colonization. The observations in RDEB patients mirrored the findings in mice. Notably, i.p. injection of collagen VII in collagen VII-deficient mice, which restored cochlin in the spleen, but not in the skin, increased systemic cochlin LCCL domain that reactivated macrophages and led to normalization of bacterial colonization of the skin. Furthermore, systemic administration of the cochlin LCCL domain was alone sufficient to decrease bacterial skin colonization in RDEB mice. Our findings uncovered the increased susceptibility to bacteria in RDEB as a consequence of systemic inability to meet bacterial challenges caused by loss of collagen VII from secondary lymphoid organs, rather than by impaired skin integrity. Furthermore, our study places focus on the lymphoid ECM as essential for maintenance of bacterial homeostasis by the host.

Results

Elevated Bacterial Colonization of RDEB Skin Is Independent on Wounding. Previous studies have suggested that RDEB is linked to increased susceptibility to colonization with *Staphylococcus aureus* (7). We first aimed to validate and extend these observations to other commensal bacteria by analysis of an independent RDEB patient cohort. Swab samples were taken from skin wound areas. All 30 analyzed patients with clinical and molecular diagnosis of severe generalized RDEB were colonized with *Staphylococcus aureus* (*SI Appendix*, Table S1). The majority were also cocolonized with other bacteria, primarily with *Streptococcus* sp. and *Pseudomonas aeruginosa* (*SI Appendix*, Table S1). Interestingly there was no apparent correlation of gender or age with bacterial burden (*SI Appendix*, Table S1), the latter indicating that the bacterial colonization in RDEB is independent of disease progression. Wounds may promote bacterial colonization; however, compared with other patients suffering from similar open wounds, RDEB patients displayed elevated bacterial colonization rates (11). These observations made us hypothesize that loss of functional collagen VII, which causes RDEB, leads to a specific dysregulation of the ability to combat bacterial challenges.

To strengthen our hypothesis, we employed the collagen VII hypomorphic mouse, which is a model of severe generalized RDEB and is thus here referred to as the RDEB mouse (1). It is particularly useful since, in contrast to human patients, the mice do not develop large wounds due to stabilization of skin by the fur (1, 23) (Fig. 1). In comparison with wild-type littermates, RDEB mice kept in a specific-pathogen–free facility, showed drastically increased bacterial burden of clinically and histologically unwounded skin (Fig. 1). Detailed analysis of the microbiome revealed that—similarly to RDEB patients—all RDEB mice were colonized with *Staphylococcus aureus*, whereas only one tested wild-type littermate showed skin colonization of this commensal pathogen (*SI Appendix*, Table S2). In addition, all RDEB mice were cocolonized with one or multiple additional bacteria (*SI Appendix*, Table S2). Furthermore, previous proteomic studies on RDEB skin had revealed a significant increase in abundance of the antimicrobial peptide Camp (3), which has been implicated to play an important role in defense against invasive *Staphylococcus aureus* infections (24). Thus, RDEB mice were able to respond to *Staphylococcus aureus* by increased production of antimicrobial peptides, yet the bacterial colonization was elevated. Collectively, this suggested a distinctly altered host response to bacteria in RDEB and led us to address the role of collagen VII in antibacterial immunity.

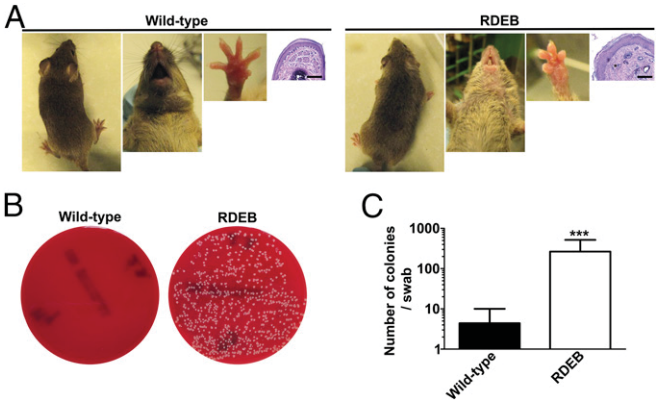

Fig. 1. Adult collagen VII-deficient mice (RDEB mice) display elevated bacterial skin colonization. (*A*) Photographs of the back, snout, and forepaws of 10-wk-old wild-type and RDEB mouse littermates and corresponding H&E staining of forepaw sections; note the absence of large wounds. (Scale bars, 100 μm.) (*B*) Blood agar plates of forepaw swab samples from the mice. (*C*) Quantification of the number of bacterial colonies per swab from wild-type and RDEB mice; $n = 8$ per group; $^{***}P = 0.0003$ (Mann–Whitney *U* test). Values represent mean ± SEM.

Collagen VII Is Present in Lymphoid Conduits in a Unique Protein Complex. Because the increased bacterial burden of RDEB skin seemed to be independent of skin integrity, we reasoned that it could result from loss of extracutaneous collagen VII. Screening of lymphoid organs for collagen VII in wild-type mice revealed high abundance in fiber-like structures in the splenic white pulp (Fig. 2*A*). RT-PCR and Western blot analyses confirmed expression of *Col7a1* mRNA (Fig. 2*B*), and synthesis of full-length collagen VII in spleen (Fig. 2*C*). PCR analysis of mRNA extracted from RDEB mouse spleens generated products corresponding to the aberrantly spliced *Col7a1* detected in this mouse model (Fig. 2*B*) (25), and Western blot analysis of protein lysates from RDEB mouse spleens showed barely detectable levels of full-length collagen VII (Fig. 2*C*), thus collectively validating the expression analysis.

To determine the identity of the collagen VII-containing fibers, we costained spleen for collagen VII, and the B- and T-cell markers, B220 and Cd3e, respectively. Collagen VII was not detected within T-cell areas but primarily present within the B-cell follicles (Fig. 2*D*). Importantly, no overlap occurred with Vegf receptor 2 staining (Fig. 2*D*), thus excluding endothelial structures. Furthermore, a MOMA-1 antibody, detecting metallophilic macrophages present in the marginal zone, revealed minimal colocalization with collagen VII, indicating that it was mostly present within the follicle. Confocal microscopy showed that the average thickness of the fiber-like structures was <1 μm, making them likely to be conduits (Fig. 3*A*). Lymphoid conduits are ECM structures composed of a collagen core surrounded by a microfibril layer and a basement membrane creating a tube (20). The molecular composition of the lymphoid conduits varies within the functionally distinct regions of the lymphoid organs (15, 20–22), suggesting that specific ECM proteins have unique functions in regulating immune reactions. Because collagen VII is linked to cells via a laminin 332–integrin α6β4 complex, we reasoned this could also occur in spleen (26–28). Indeed, collagen VII, laminin 332, and integrin α6β4 colocalized in the white pulp (*SI Appendix*, Fig. S1). These analyses suggest that collagen

http://doc.rero.ch

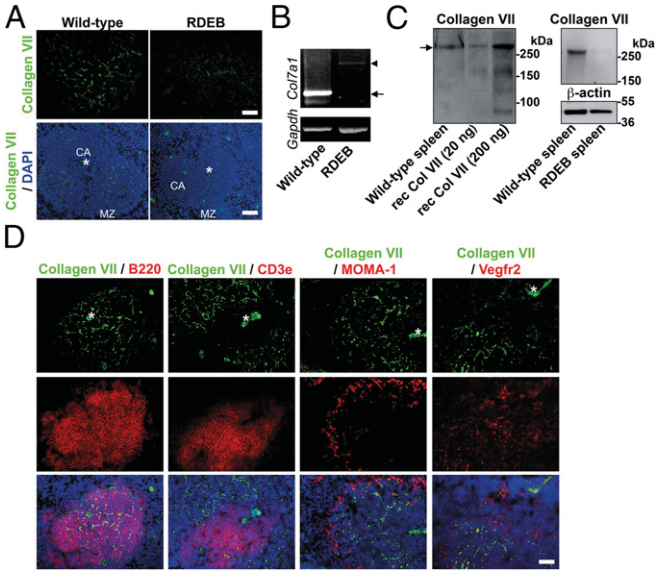

Fig. 2. Collagen VII is expressed in the spleen. (*A*) Wild-type and RDEB mouse spleen stained for collagen VII (green). [Scale bars: 50 μm (*Top*); 100 μm (*Bottom*).] The positions of the central arteriole (CA) and marginal zone (MZ) are indicated. (*B*) RT-PCR for *Col7a1* and *Gapdh* on RNA extracted from wild-type and RDEB mouse spleens as indicated. Arrow points to wild-type transcript, and arrowhead to aberrantly spliced *Col7a1* transcript in RDEB mice (25). (*C*, *Left*) Western blot analysis of collagen VII in wild-type mouse spleen lysates; 20 and 200 ng of recombinant human collagen VII were run in parallel lanes. Arrow points to full-length collagen VII. (*C*, *Right*) Western blot analysis of wild-type and RDEB mouse spleen lysates for collagen VII and β-actin as loading control. (*D*) Immunofluorescence analysis of codistribution of collagen VII (green), with B220 (B cells, red), Cd3e (T cells, red), MOMA-1 (red), and Vegf receptor 2 (Vegfr2) (red), respectively. (Scale bar, 100 μm.) Nuclei visualized with DAPI (blue). Asterisks indicate central vessels visible by autofluorescence.

VII in spleen is part of a unique multiprotein complex, similar to complexes normally found at the dermal–epidermal junction zone in skin.

Next, by using confocal microscopy, we determined the localization of collagen VII within lymphoid conduits more precisely. Comparative analysis of laminin α5—a component of the basement membrane in lymphoid conduits (20)—with laminin 332 and collagen VII revealed collagen VII on the luminal side and arranged around the lumen. Laminin α5 and laminin 332 overlapped and surrounded collagen VII on the outside (Fig. 3*B* and *SI Appendix*, Fig. S2*A*). To validate the analysis, we stained conduits in the T-cell area for laminin α5 and collagen I. This subset of conduits was chosen as they are known to contain a distinct collagen core composed of collagen I (21, 29). Indeed, a clear collagen core surrounded by laminin α5-containing laminins was visible (*SI Appendix*, Fig. S2*A*). As additional means to determine the localization of collagen VII in lymphoid conduits, we made use of the fact that splenic conduits are connected to the vasculature and conduct circulating fluids and small particles (14). We systemically injected 10-kDa FITC-labeled dextran in wild-type mice. Ten minutes after injection, spleens were removed, fixed, and sectioned. Staining with collagen VII revealed that FITC-positive particles were clearly present within a space bordered with collagen VII (Fig. 3*C*). Collectively, our studies suggest that collagen VII is strongly present in the microfibrillar layer of lymphoid conduits (Fig. 3*B* and *SI Appendix*, Fig. S2*A*).

Collagen VII Is Expressed by Lymphoid Stromal Cells. Given the abundance of collagen VII in a subset of splenic conduits, it was important to identify its cellular source. Lymphoid conduits are decorated with distinct types of stromal cells (20, 21). αSMA-positive fibroblastic reticular cells (FRCs) and the ER-TR7 antigen both identify T-cell zone conduits, whereas lactadherin (Mfge8) and C1q identify follicular dendritic cells (FDCs), which are associated with follicular conduits (30, 31). Immunofluorescence analysis revealed only limited overlap of collagen VII with αSMA or ER-TR7 in spleen (*SI Appendix*, Fig. S2 *B* and *D*), but close association with Mfge8- and C1q-positive FDCs (*SI Appendix*, Fig. S2 *C* and *D*). We then isolated stromal cells from spleen and expanded them in vitro. In these cultures, which were devoid of leukocytes and lymphocytes, as indicated by absence of *Cd45*, *Cd3e*, and *Cd19*, but maintained expression of FRC and FDC markers (Fig. 3*D*), ample *Col7a1* expression was detected in wild-type cells (Fig. 3*D*). In contrast, only aberrantly spliced *Col7a1* transcripts were detected in cells isolated from the spleen of RDEB mice (Fig. 3*D*). Taken together, we concluded that collagen VII is a unique, stromal cell-derived component that in spleen is primarily found in follicular conduits.

Collagen VII Physically Interacts with the Innate Immune Activator Cochlin. We were intrigued by the presence of collagen VII in lymphoid conduits and strived to understand its function. The previously reported elevated humoral immunity in RDEB (32, 33), together with the observation that the T-cell areas in spleen were devoid of collagen VII, suggested that absence of collagen VII may cause a specific impairment of innate antibacterial immunity. In the conduit basement membrane, collagen VII would interact with laminin 332 and collagen IV (*SI Appendix*, Figs.

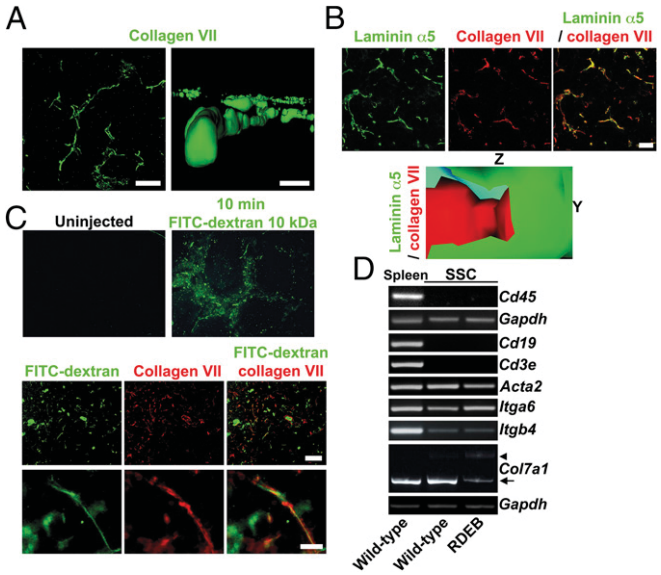

Fig. 3. Collagen VII is part of lymphoid conduits. (*A*) Confocal analysis of splenic collagen VII structures (green). On the *Left* side is an *XY* projection, and the *Right* side shows a computed *YZ* 3D rendition. [Scale bars: 10 μm (*Left*); 1 μm (*Right*).] (*B*, *Top*) Maximum intensity projection of confocal *Z* stack of splenic follicle stained for laminin α5 (green) and collagen VII (red). (Scale bar, 10 μm.) (*B*, *Bottom*) A longitudinal cut, applied through computed 3D model of confocal *Z*-stack scans, shows collagen VII to be located inside the laminin α5-containing conduit basement membrane. The *Y* and *Z* axes are displayed as indicated. (*C*) Images of spleen sections from a wild-type mouse 10 min after systemic injection of 10-kDa FITC-dextran (green) stained for collagen VII (red). (Scale bars, 5 μm.) (*D*) RT-PCR analysis of mRNA from wild-type spleen, or cultured SSCs from wild-type or RDEB mice for *Cd45*, *Cd19*, *Cd3e*, *Acta2*, *Itga6*, *Itgb4*, *Col7a1*, and *Gapdh* transcripts. Absence of *Cd45*, *Cd19*, and *Cd3e* transcripts confirms cultures to be devoid of leukocytes and lymphocytes. Presence of *Itgb4* transcript indicates follicular dendritic cells in the cultures (*SI Appendix*, Fig. S2) (31). Arrow points to wild-type *Col7a1* transcript, and arrowhead to aberrantly spliced *Col7a1* transcript (25).

http://doc.rero.ch

S1 and S2*A*) (22, 34), but the luminal interaction partners remained elusive. Relatively few proteins have been described to be present in the lumen of lymphoid conduits. An unexpected insight came from unrelated proteomic analysis of mouse paws (*SI Appendix*, Fig. S3). We noted that the abundance of the ECM protein cochlin was drastically diminished in RDEB mouse paws (*SI Appendix*, Fig. S3). This sparked our interest because, in response to bacterial infection, aggrecanase-mediated processing of cochlin releases its LCCL domain into the circulation. The released LCCL domain activates macrophages and neutrophils, stimulating bacterial clearance (16). Cochlin was also of particular relevance as it directly interacts with collagens (35). Importantly, spleens from RDEB mice displayed elevated aggrecanase-1 and -2 expression (*SI Appendix*, Fig. S4). In accordance with previous studies (16), we detected aggrecanase-2 in spleen as the major aggrecanase with cochlin-processing capability. However, in contrast to the previous study, aggrecanase-2 was also dramatically increased in bacterially colonized RDEB mice (*SI Appendix*, Fig. S4), suggesting a difference in the response of aggrecanase-1 and -2 expression to acute infection vs. chronic bacterial colonization. Costaining of collagen VII and cochlin revealed that, indeed, cochlin was coexpressed with collagen VII in splenic conduits (Fig. 4*A*).

Of the collagens known to bind cochlin, only collagen IV is present in splenic follicular conduits and colocalizes with collagen VII in these structures (*SI Appendix*, Fig. S5) (21, 29). However, our protein–protein binding assays showed that, in addition to collagen IV, cochlin bound collagen VII in a saturable manner (Fig. 4*B*). The binding to collagen VII was slightly but significantly stronger than to collagen IV (K_d, 46 ± 8 and 79 ± 22 nM, respectively; $^{**}P = 0.0062$) (Fig. 4*B*). Direct interaction between collagen VII and cochlin was confirmed by coimmunoprecipitation of spleen lysates and splenic stromal cell-conditioned medium (*SI Appendix*, Fig. S6).

Next, we wanted to determine the interaction of collagen VII with cochlin in more detail. Cochlin has one LCCL domain and two VWFA domains; the C-terminal VWFA2 domain has been shown to interact with collagens including collagen IV (35). We cloned and expressed the LCCL, VWFA1, and two domains (*SI Appendix*, Fig. S7), and investigated their ability to interact with collagen IV and VII. In solid-phase assays on immobilized cochlin domains, neither collagen IV nor collagen VII interacted with the LCCL domain in a saturable manner (Fig. 4*C*). The binding to both VWFA domains reached saturation for both collagens, but with different patterns. Collagen IV interacted stronger with the VWFA2 domain than with the VWFA1 domain (K_d to VWFA1, 64 ± 10 nM, vs. K_d to VWFA1m, 49 ± 13 nM; $P = 0.40$). In contrast, collagen VII interacted significantly stronger with the cochlin VWFA1 domain than with the VWFA2 domain (K_d to VWFA1, 17 ± 7 nM, vs. K_d to VWFA2, 54 ± 8 nM; $^{*}P = 0.013$) (Fig. 4*C*). Collectively, our results extend previous findings (35) and indicate a model in which the different affinities of collagen IV and collagen VII to the cochlin VWFA domains establish directionality of cochlin in the conduits, and position the cochlin LCCL domain toward the conduit lumen (Fig. 4*D*). This enables rapid systemic release of the LCCL domain after aggrecanase-1– and -2–mediated proteolysis.

Collagen VII Is Indispensable for Retention of Cochlin in Lymphoid Conduits. Next, we took advantage of the highly time-specific postnatal expansion of the splenic T-cell zone and B-cell follicle that occurs in rodents, to gain more insight into the relationship of collagen VII and cochlin. Immediately after birth, B cells accumulate around central vessels in spleen (36). Splenic B-cell follicles become recognizable during the second and third week of life, and in lymph nodes remodeling of existing conduits in areas previously occupied by T cells has been shown to contribute to formation of follicular conduits (22, 37). Immunofluorescence analysis revealed that deposition of collagen VII in spleen was readily visible 20 d after birth and reached mature appearance 40 d after birth (Fig. 4*E*). Interestingly, cochlin deposition mirrored the temporal and spatial pattern of collagen VII expression (Fig. 4*E*), suggesting a close functional relationship. In spleens of the RDEB mice, the general architecture of follicles, as visualized by laminin α5 staining, did not differ from that of wild type. However, deposition of both collagen VII and cochlin in follicles between 20 and 40 d was significantly reduced, compared with wild-type spleens (Fig. 4*E*). Western blotting confirmed clearly diminished cochlin abundance in the spleen of adult RDEB mice, with only 61 ± 12% cochlin being present compared with wild-type spleen (Fig. 4*F*). However, reduction of collagen VII did not reduce *Coch* transcripts (Fig. 4*G*) or cochlin synthesis in cultured splenic stromal cells (*SI Appendix*, Fig. S8). Taken together, the data suggest that collagen VII is crucial for physical retention of cochlin in splenic conduits.

Cochlin is also expressed in other secondary lymphoid organs (16). To establish a generality of our findings for other secondary lymphoid organs, we isolated mandibular lymph nodes from wild-type and RDEB mice and used immunohistochemical and biochemical methods to characterize them. Indeed, collagen VII was present with cochlin in lymphoid conduits (*SI Appendix*, Fig. S9 *A*–*C*). However, the distribution of both proteins was slightly different from spleen, and collagen VII and cochlin were also found outside the B-cell areas, pointing to potentially divert and additional functions of the collagen VII–cochlin complex in spleen and lymph nodes. Importantly, cochlin was also significantly reduced in RDEB mouse lymph nodes (*SI Appendix*, Fig. S9 *C* and *D*). Western blots of whole-lymph node protein extracts confirmed the immunohistological analyses (*SI Appendix*, Fig. S9*E*). Given that lymph nodes would largely be involved in maintaining regional immunity and spleen would to a greater extent support systemic immunity, we focused our following studies on spleen.

To conclusively demonstrate that retention of cochlin in lymphoid conduits depended on collagen VII, we systemically ablated *Col7a1* expression in a tamoxifen-inducible *Col7a1* knockout mouse (1). In accordance with the previously established half-life of collagen VII (38), tamoxifen treatment led to a significant loss of collagen VII in skin and spleen after >10 wk (Fig. 5 *A* and *B*). Notably, cochlin was concomitantly lost from spleen in a manner that paralleled collagen VII abundance (Fig. 5 *B* and *C*). Remarkably, ablation of collagen VII, with concurrent loss of cochlin from spleen, promoted bacterial colonization of skin (Fig. 5 *D* and *E*). Furthermore, there was a good negative correlation with collagen VII abundance and bacterial colonization of the skin (Fig. 5*F*). It is important to point out that this effect was achieved in absence of, and preceded, significant breach of skin integrity (Fig. 5*A*) (38).

The Lymphoid Collagen VII–Cochlin Axis Maintains Bacterial Colonization Homeostasis of Skin. We next sought to determine the immunological relevance of the above findings. Loss of cochlin as a consequence of collagen VII deficiency in lymphoid conduits suggested that RDEB patients with missing or abnormal collagen VII are unable to increase circulating levels of the macrophage- and neutrophil-stimulating cochlin LCCL domain during bacterial infections. Toward this end, we first analyzed sera from patients with severe generalized RDEB and patients with infected chronic wounds due to venous insufficiency (non-RDEB); all patients in both groups had at least one acutely infected wound. Healthy volunteers with no localized or systemic infection served as controls. Western blotting of the sera with a monoclonal antibody raised against the LCCL domain showed, as expected, that the LCCL domain was strongly increased in non-RDEB patients with infected wounds, compared with controls. In contrast, individuals with RDEB and infected wounds were unable to mount such response (Fig. 6 *A* and *B*).

To assess the effect on macrophage activity, we analyzed biopsies taken from infected skin wounds. Importantly, despite a

http://doc.rero.ch

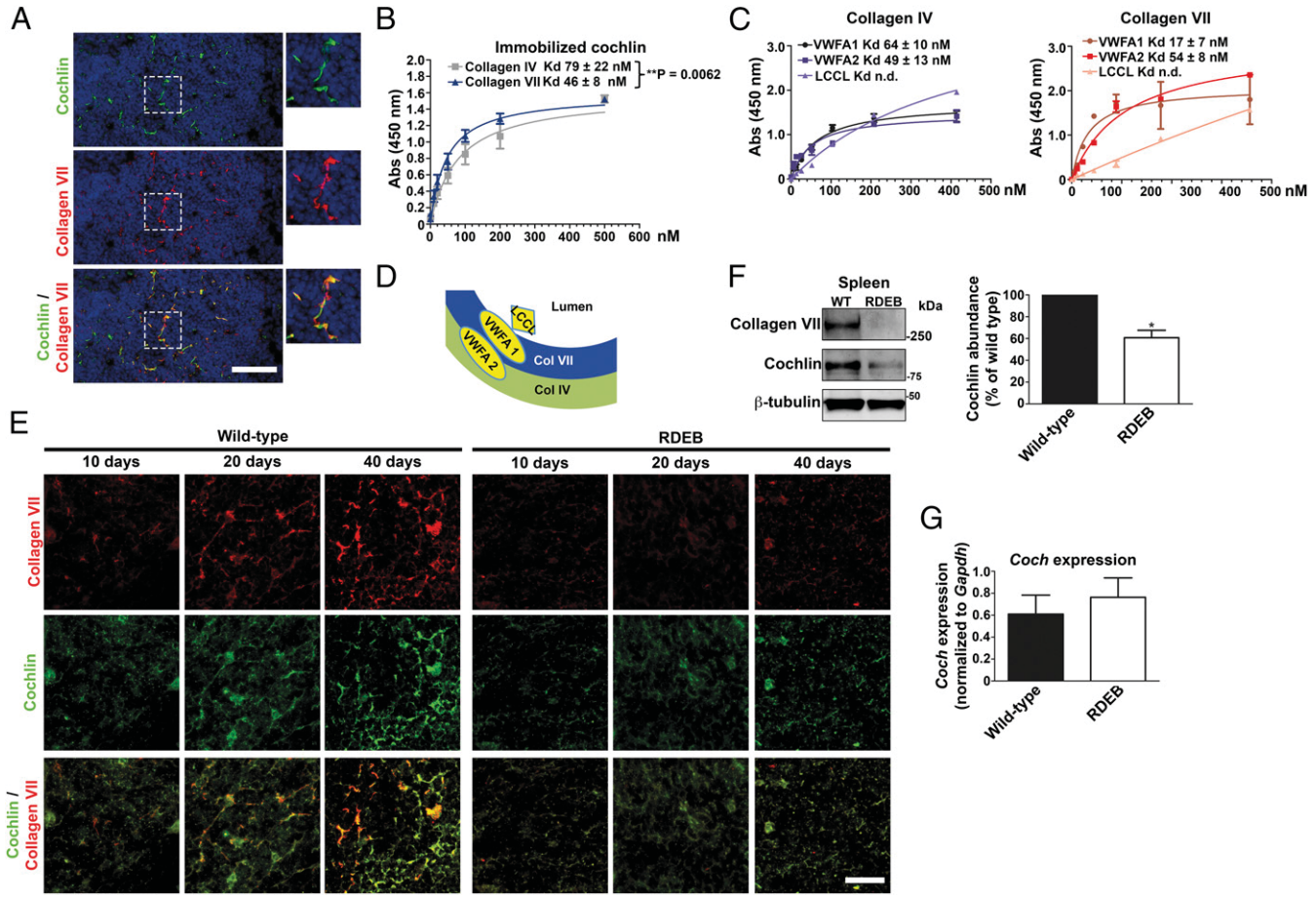

Fig. 4. Collagen VII interacts with cochlin and is indispensable for cochlin deposition in splenic follicular conduits. (*A*) Immunofluorescence staining of adult wild-type mouse spleen for cochlin (green) and collagen VII (red). (*B*) Solid-phase binding assay of immobilized human cochlin to human collagen IV (gray squares) and human collagen VII (blue triangles). (*C*) To test the interaction with the cochlin LCCL, VWFA1, and VWFA2 domains, 100 ng of purified recombinant murine cochlin LCCL, VWFA1, or VWFA2 domain were immobilized on microtiter plates and overlaid with increasing concentrations of human collagen VII or collagen IV. Shown are the binding curves and K_d for collagen IV and VII calculated from four experiments. (*D*) A schematic model of cochlin interactions and position in lymphoid conduits. (*E*) Staining of spleen from 10-, 20-, and 40-d-old wild-type and RDEB mice, as indicated. Due to the species used for the collagen VII (red) antibody and the fact that the cochlin LCCL domain may be released, a goat polyclonal antibody detecting the cochlin VWFA domains (green) was used for this and all subsequent double stainings with collagen VII. (*F*) Western blot on adult wild-type or RDEB mouse spleen lysates, probed for collagen VII, cochlin (rabbit polyclonal antibody), and β-tubulin (*Left*). Densitometric quantification of three blots; cochlin expression normalized to β-tubulin and expressed as percentage of wild type; $*P = 0.0293$ (*Right*), significance tested with paired Student's *t* test. (*G*) qPCR analysis of *Coch* expression in adult wild-type or RDEB mouse spleen. Values were normalized to *Gapdh*. Wild-type vs. RDEB mouse, $P = 0.5458$, significance tested with unpaired Student's *t* test. All values represent mean ± SEM.

generally increased expression of IL-6 in RDEB wounds (3), the specific IL-6 response in macrophages was substantially hampered, compared with non-RDEB wounds (Fig. 6*C*). These data suggest a systemic inability to respond adequately to bacterial challenges in RDEB owing to the loss of collagen VII–cochlin interaction in secondary lymphoid organs.

The mechanisms by which the cochlin LCCL domain activates innate immune cells still remain elusive. Therefore, we treated serum-starved mouse macrophage RAW 264.7 cells with 0.3 μg/mL recombinant mouse LCCL domain. Western blotting of cell lysates revealed a transient increase in tyrosine phosphorylation of distinct proteins after 5- and 30-min treatment (*SI Appendix*, Fig. S10). This result suggests, in contrast to previous observations (16), a direct rather than an indirect macrophage-activating effect of the LCCL domain.

The cochlin abundance in wild-type mouse skin was low when detected by proteomics and undetectable by Western blot analysis. Therefore, dermal deposits of cochlin were not likely to play a major part in antibacterial response. Nevertheless, it was important to exclude this and confirm the role of lymphoid collagen VII–cochlin axis in regulation of innate immunity. Toward this end, we aimed to restore collagen VII in spleen of RDEB mice. Previous work has shown that part of i.v. injected collagen VII can reach wounded skin and be deposited in the dermal–epidermal junction zone (39). We reasoned that i.p. injected collagen VII (900 kDa) would likely be too large to be systemically distributed, and that this mode of administration could lead to efficient targeting of spleen. Twenty micrograms of recombinant human collagen VII was i.p. injected, close to the spleen. One week after injection, the first control was to test the skin. Using both human collagen VII-specific antibodies (40) and antibodies detecting both human and murine collagen VII, we found no deposition of the injected collagen VII in skin by immunofluorescence staining or Western blot analysis (*SI Appendix*, Fig. S11 *A* and *B*). Functionally, there was no evidence of increased skin stabilization; skin from RDEB mice injected with collagen VII still readily separated from forces applied during sectioning (*SI Appendix*, Fig. S11*C*). On the contrary, de novo deposition of human collagen VII was detected in splenic B-cell follicles by using an antibody recognizing human but not murine collagen

http://doc.rero.ch

VII (Fig. 7*A*). Western blot analysis confirmed presence of full-length human collagen VII in spleen (*SI Appendix*, Fig. S11*D*). Although the distribution pattern was more diffuse than in wild-type spleen, the newly introduced collagen VII promoted retention of cochlin (Fig. 7*B*), which was also affirmed by Western blotting detecting significantly increased levels of cochlin in spleens from RDEB mice injected with recombinant collagen VII (*SI Appendix*, Fig. S11 *D* and *E*). Our analyses did not exclude deposition of the injected collagen VII in lymph nodes or other organs, apart from skin. Importantly, the analyses also revealed highly increased levels of circulating cochlin LCCL domain (Fig. 7C) and reactivation of previously quiescent skin-resident Cd11b-positive neutrophils and macrophages, as indicated by increased levels of IL-1β and IL-6 (Fig. 7 *D* and *E*). To further corroborate the activation of innate immunity after restoration of collagen VII in spleen but not skin, we analyzed circulating levels of IL-1β and IL-6. Importantly, the levels of both cytokines were clearly increased 1 wk after injection of collagen VII, indicative of a systemically elevated antibacterial response (Fig. 7*F*).

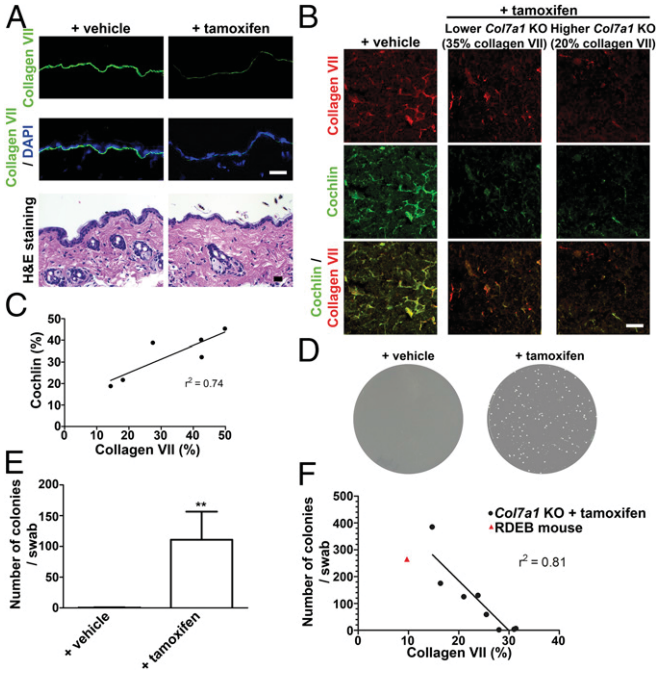

Fig. 5. Ablation of collagen VII in adult mice leads to loss of cochlin from spleen and increased bacterial skin colonization before affecting skin integrity. (*A*) Back skin from tamoxifen-inducible *Col7a1* knockout mice 12 wk after injection with tamoxifen or corn oil (vehicle). (*Top* and *Middle*) Sections stained for collagen VII (green) and nuclei visualized with DAPI (blue). (*Bottom*) H&E staining showing no apparent dermal–epidermal separation in vehicle- or tamoxifen-treated mice. (Scale bars, 100 μm.) (*B*) Spleen from tamoxifen-inducible *Col7a1* knockout mice and controls 12 wk after knockout induction. Sections stained for collagen VII (red) or cochlin (green, goat polyclonal antibody), as indicated. Shown are a low responder (35% residual collagen VII compared with vehicle-treated controls) and a high responder (20% residual collagen VII compared with vehicle-treated controls), as determined by ImageJ-based quantification of antibody staining intensity for collagen VII on five spleen sections (38). (Scale bars, 100 μm.) (*C*) Plot of collagen VII abundance vs. cochlin abundance quantified by immunofluorescence staining as described in *B*. Linear regression analysis reveals a good correlation ($r^2 = 0.74$) of collagen VII vs. cochlin content. (*D–F*) Ablation of collagen VII in adult mice results in increased bacterial colonization. Bacterial swabs from forepaws of mice treated as in *A*. (*D*) Photos of representative LB-agar plates. (*E*) Quantification of number of bacterial colonies per plate; $n = 8$; $^{**}P = 0.0015$, significance tested with Mann–Whitney *U* test. Values represent mean ± SEM. Five tamoxifen-treated mice showed highly and three slightly increased bacterial colonization, virtue of different knockout efficiency. (*F*) Plot of collagen VII abundance vs. bacterial colonies. Linear regression analysis reveals a good negative correlation ($r^2 = 0.81$) of collagen VII abundance vs. bacterial colonies.

The ultimate functional outcome of the reinstatement of the collagen VII–cochlin interaction in spleen and potentially other secondary lymphoid organs was rapid and potent resolution of the bacterial supercolonization of collagen VII-deficient skin (Fig. 8 *A* and *B*). Macroscopic and histopathological analyses showed no overt benefit of the collagen VII injections on improving the skin stability (Fig. 8*A* and *SI Appendix*, Fig. S11*C*). Even in mice with severely progressed RDEB, as exemplified by a 40-wk-old mouse (Fig. 8*A*), restoration of collagen VII-mediated retention of cochlin in spleen and potentially other secondary lymphoid organs dramatically reduced the bacterial colonization of skin (Fig. 8 *A* and *B*). To conclusively support the causal link of reduction of circulating levels of the cochlin LCCL domain and increased bacterial colonization of skin in RDEB, we systemically administered affinity-purified murine recombinant cochlin LCCL domain in RDEB mice on 2 consecutive days (Fig. 8*C*). The LCCL domain-treated RDEB mice responded with a rapid and significant decrease in bacterial colonization 2 d after the last injection. The benefit of the LCCL domain was sustained; bacterial colonies were further decreased 5 d after the last injection (Fig. 8*C*). Collectively, the rescue experiments validated the interrupted collagen VII–cochlin axis as the major cause for increased bacterial colonization in RDEB, and revealed a multiprotein complex including collagen VII and cochlin as a systemic supporter of innate immune-mediated bacterial defense.

Discussion

Here, we provide an unexpected explanation for the increased susceptibility to bacterial colonization of skin and nasal cavities in RDEB. We show that this is not—as previously believed—a consequence of loss of collagen VII from mucocutaneous surfaces but is caused by loss of collagen VII from the secondary lymphoid organs. This results in an inability to sustain proper systemic control over innate immunity in response to bacterial challenges.

Although RDEB has so far been primarily viewed as a skin disorder, individuals with RDEB show frequent extracutaneous involvement. Collagen VII is—besides skin and mucosa—present in the ECM of multiple organs, but its functions in these organs remain to be addressed. For example, during dental development, collagen VII plays a direct instructive role (41), indicating that it fulfils vital, nonredundant functions in extracutaneous tissues. Our discovery of the role of collagen VII as an important interactor of cochlin and provider of its directionality in secondary lymphoid organs supports this notion. Collagen VII is a regulator of innate immunity, and this, by extension, shifts the view of RDEB from a mucocutaneous disease to a systemic disorder with multiorgan involvement.

However, it has to be stressed that collagen VII deficiency in skin alone may have widespread consequences, which include localized dysregulation of TGFβ bioavailability and inflammation promoted by tissue damage (2, 3). Thus, it can be expected that other immune cells and their respective antibacterial functions are also affected by RDEB. Nevertheless, and notably, our data point to the collagen VII–cochlin axis as being a major supporter of dermal and systemic antibacterial immunity.

It is widely accepted that, apart from the structural deficiencies, the pathology of different ECM disorders involves a broad spectrum of complex biological mechanisms, such as endoplasmic reticulum stress, dysregulated autophagy, or altered bioavailability of biologically active peptides and factors (42–46). Here, we demonstrate that this is also the case for RDEB. The functional role of individual ECM proteins as lymphoid conduit components has not been appreciated, perhaps because mutations in their genes often cause severe mucocutaneous phenotypes that may overshadow their deficiency in other organs (34). Indications exist that also defects in other basement membrane

http://doc.rero.ch

proteins may be associated with increased susceptibility to bacterial colonization (47).

A pertinent question in the context of skin fragility disorders, such as RDEB, is whether wounds alone could be a sufficient reason for increased bacterial colonization of the host. We addressed this question in conditional collagen VII knockout mice and showed that, upon collagen VII ablation, increased bacterial colonization precedes reduced skin integrity and wounds. This strongly indicates that the breakdown of the collagen VII–cochlin axis and the subsequent loss of control over systemic regulation of innate immunity is the primary cause of increased susceptibility to bacteria in RDEB.

The loss of cochlin from collagen VII-deficient secondary lymphoid organs despite presence of collagen IV indicates that dual interactions with collagen IV and collagen VII or, alternatively, interactions with collagen VII alone, are essential for optimal retention and/or structural organization of cochlin in lymphoid conduits. Dual interactions with collagen IV and VII would allow correct luminal presentation of the cochlin LCCL domain (Fig. 4*D*). However, although cochlin was reduced in collagen VII-deficient spleen and lymph nodes, it was not decreased to the same extent as collagen VII. This, together with the incomplete overlap of collagen VII and cochlin deposition, implies that cochlin and collagen VII likely also have functions in the secondary lymphoid organs that are not strictly dependent on each other. Given the location of both proteins in the lumen of conduits, they could regulate the physical properties of the conduits, for example, the flow of liquids and particles (16).

The mechanism by which the LCCL domain of cochlin activates innate immune cells remains elusive. We provide some support for a direct signaling function of the LCCL domain. However, a potential receptor on macrophages and neutrophils, and the downstream signaling mechanism remain to be identified. Furthermore, no help has been provided by genetic defects

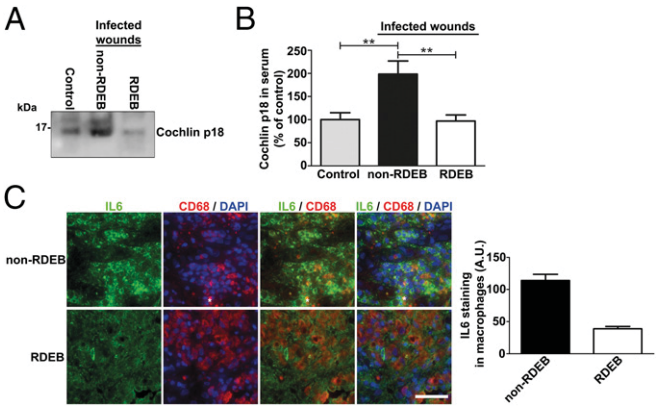

Fig. 6. The innate immunity-regulating collagen VII–cochlin axis is broken in RDEB. (*A*) Western blot of sera from a healthy donor (control), a donor with a bacterially infected chronic wound (non-RDEB), and a donor with RDEB with infected wounds (RDEB). Five microliters of serum was loaded per lane on 15% tricine gels, and blots probed for cochlin with a monoclonal antibody detecting the released LCCL domain (p18 fragment as indicated) (rat anti-cochlin clone 9A10D2). (*B*) Densitometric quantification of bands as in *A*, values expressed as the percentage of the levels in the control group. Values represent mean ± SEM; $n = 6$; control vs. non-RDEB, $^{**}P = 0.0051$; RDEB vs. non-RDEB, $^{**}P = 0.0032$; control vs. RDEB, $P = 0.88$. Significance tested with unpaired t test with Welch's correction. (*C*, *Right*) Wound granulation tissue from infected non-RDEB and RDEB wounds, stained for IL-6 (green), CD68 (red), and DAPI (blue). Note that, despite the generally increased expression of IL-6 in RDEB wounds (3), its expression in CD68-positive macrophages is significantly lower in RDEB wounds. (Scale bar, 100 μm.) (*C*, *Left*) Quantification of the intracellular staining intensity of IL-6 in CD68-positive cells (macrophages).

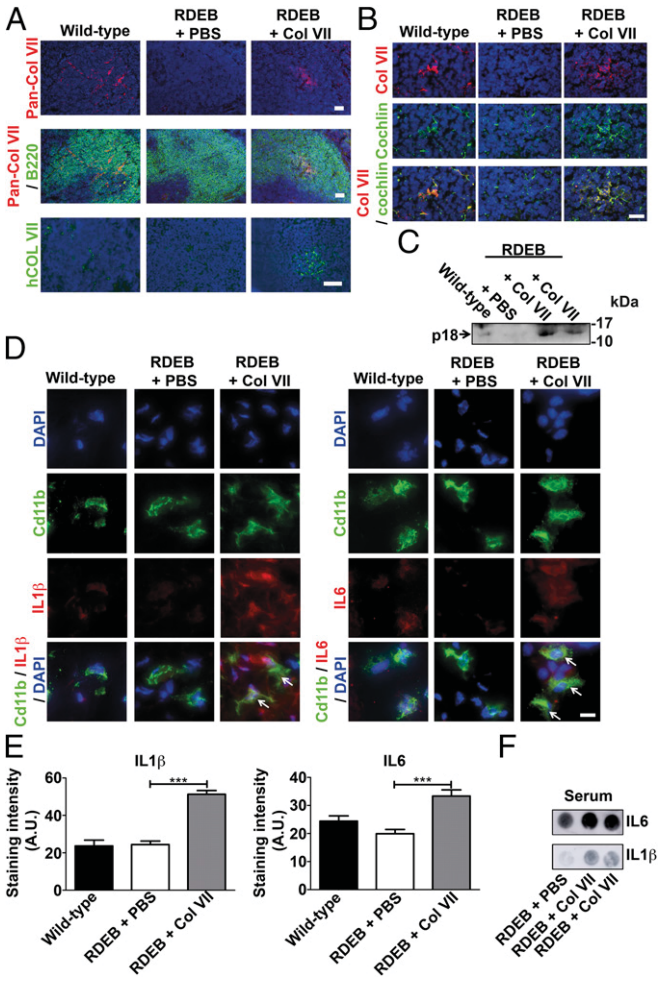

Fig. 7. Restoration of the collagen VII–cochlin axis increases circulating levels of cochlin LCCL domain and activates neutrophils and macrophages in skin. (*A–F*) Wild-type and RDEB mice were injected i.p. with either PBS or 20 μg of human recombinant collagen VII 1 wk before sample collection. (*A*) Spleen stained for pan-collagen VII (red) and B220 (green) or human collagen VII (40, green). (Scale bar, 50 μm.) (*B*) Spleen stained for cochlin (goat polyclonal, green) and collagen VII (red). (Scale bar, 20 μm.) (*C*) Western blot of serum (8 μL per lane) probed for cochlin; the arrow shows the released cochlin LCCL domain (p18 fragment, rat anti-cochlin clone 9A10D2 used) (18). (*D*) High magnification of skin stained for Cd11b (green) and IL-1β (red) or IL-6 (red). Arrows indicate activated IL-1β– or IL-6–positive macrophages. (Scale bar, 5 μm.) (*A*, *B*, and *D*) Nuclei visualized with DAPI (blue). (*E*) Quantification of the intracellular staining intensity of IL-1β and IL-6 in Cd11b-positive cells; $n > 100$ cells quantified per group; $^{***}P < 0.0001$ (unpaired Student's t test). (*F*) Dot blots of 5 μL of serum from one PBS-injected and two collagen VII-injected RDEB mice probed for IL-1β and IL-6. Note the clear increase of IL-1β and IL-6 in the sera from collagen VII-injected RDEB mice, indicating an elevated systemic antibacterial response.

that often indirectly increase the understanding of physiological functions of proteins. Only very few *COCH* mutations have been discerned so far (19); most of them are gain-of-function mutations and cause progressive deafness as a primary phenotype.

Delineating the molecular physiology and pathomechanisms of cochlin will be useful for designing unique antibacterial treatments that do not contribute to drug resistance of bacteria. To activate host cells rather than to target bacteria seems an attractive approach. In regard to utilizing the innate immune regulating collagen VII–cochlin axis for therapeutic purposes, different approaches seem possible, for example, selectively stimulating aggrecanase-1 and -2 activity and the release of the

http://doc.rero.ch

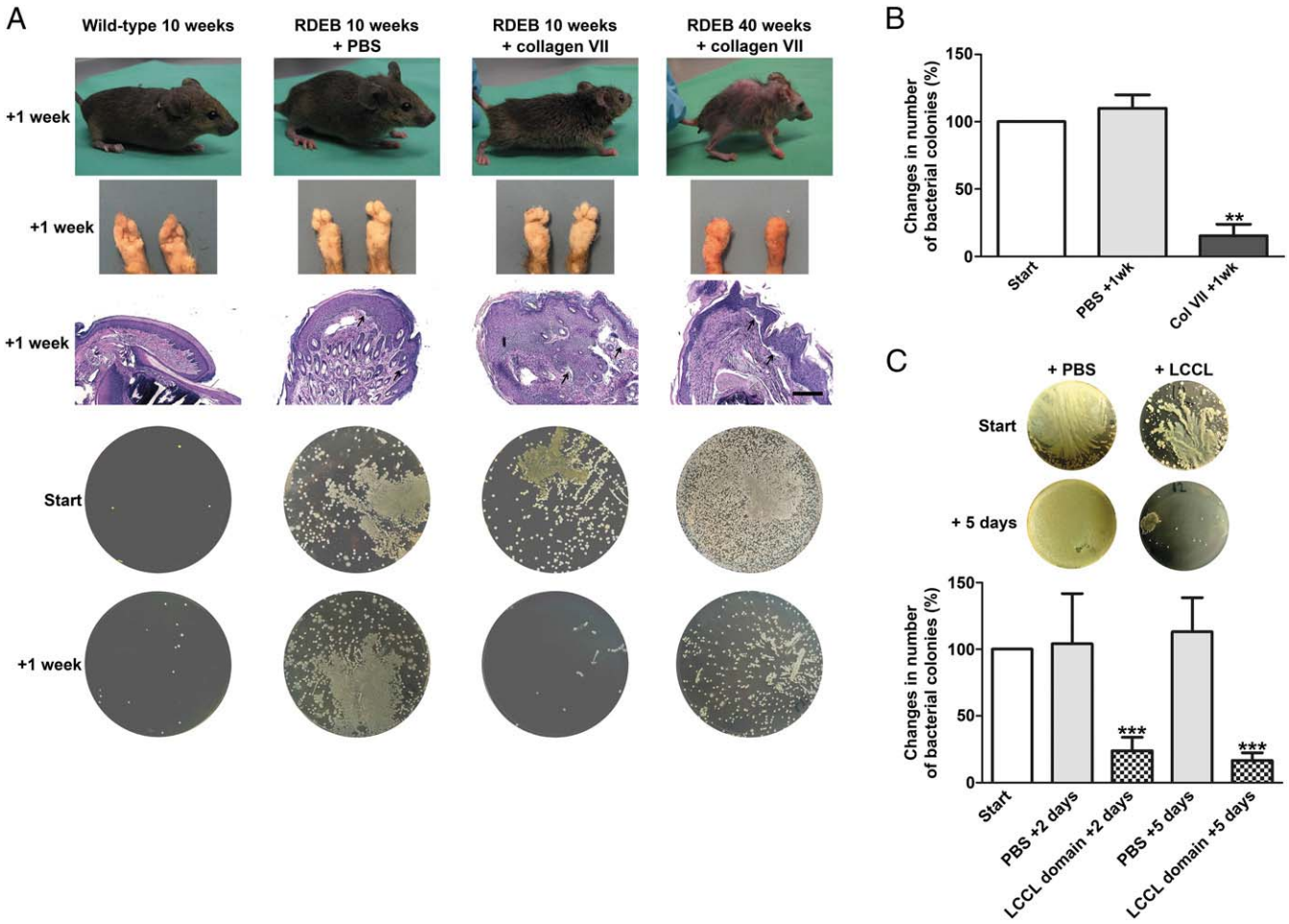

Fig. 8. Restoration of the collagen VII–cochlin axis reduces skin bacterial load. (*A*) Photographs of sampled mice, their forepaws, H&E-stained paraffin sections of their forepaws, and corresponding LB-agar plates. Note the epidermal dermal separation in the histological specimens of all PBS and collagen VII-treated RDEB mouse forepaws (arrows), indicating persisting skin fragility. (Scale bar, 100 μm.) The deformities of the paws at 40 wk are due to progressive soft tissue fibrosis in RDEB and develop with advancing course of the disease. Forepaws were swabbed just before and 1 wk after i.p. injection with PBS or 20 μg of collagen VII. (*B*) The percentage change in colonies in RDEB mice 1 wk after injection with PBS or collagen VII; $n > 4$; $^{**}P = 0.0023$ (paired Student's *t* test). Values represent mean ± SEM. (*C*, *Top*) Representative LB-agar plates from swab samples taken from RDEB mice before and 5 d after the last i.p. injection with PBS or the cochlin LCCL domain. (*C*, *Bottom*) The percentage change in colonies in RDEB mice 2 or 5 d after injection with PBS or cochlin LCCL domain. Swab samples collected as in *A*. Values represent mean ± SEM; $n = 6$ per group; $^{***}P < 0.0001$ (paired Student's *t* test).

cochlin LCCL domain, or topical application of recombinant LCCL peptide to infected areas, or design of small molecules that activate a putative LCCL domain receptor or its downstream signaling.

Taken together, our study promotes a shift of the view of RDEB as a mucocutaneous blistering disorder to a systemic disease with multiorgan involvement, identifies unique mechanisms of action of collagen VII in secondary lymphoid organs, and opens perspectives for biologically valid therapies based on the collagen VII–cochlin axis. Furthermore, it underlines the role of the ECM as a controller of immunity. The lymphoid ECM can no longer be viewed as a passive scaffold that frames immune cell interactions, but rather it is a dynamic instructive unit and active regulator of immunity.

Materials and Methods

Study Design. The underlying cause of the highly increased bacterial colonization of skin and nasal cavities in patients suffering from severe RDEB was investigated. For the studies, samples from human individuals with molecularly confirmed severe generalized recessive RDEB were used, as well as two genetic mouse models, the collagen VII hypomorphic RDEB mouse and a tamoxifen-inducible *Col7a1* knockout mouse (1). The RDEB mouse shows all major signs of severe RDEB (25), and the tamoxifen-inducible *Col7a1* knockout mouse allows targeted ablation of *Col7a1* expression in time and space (1). RDEB is a progressive disease. To obtain detailed information of bacterial colonization in relation to disease progression, we sampled individuals with RDEB of different ages, from 3 to 67 y old. Due to having more male patients in our cohort, more male than female patients were analyzed. The studies using the RDEB mouse aimed to confirm the finding in human patients, and accordingly we used mice of different ages, from 6 wk, representing intermediately progressed RDEB, to 22 wk, representing severely progressed RDEB. For these analyses, we used an equal number of female and male mice to account for potential gender-specific responses. The timing of swab sample collection in tamoxifen-inducible *Col7a1* knockout mice after *Col7a1* ablation and in RDEB mice after collagen VII injections, was chosen based on knowledge of collagen VII tissue half-life and the dynamic of collagen VII deposition at the dermal–epidermal junction zone after delivery into tissue (38). Sample size was estimated on the variance from initial analysis by performing a log-rank test with a power of 80% and for a value of $P < 5\%$. Due to the high lethality of the RDEB mouse, some experiments had to be run sequentially with a lower number of mice in each group than calculated by the sample size estimation. However, for the experiments, all groups were still included for every run. Data collection was stopped once the sample size had reached the estimated number. Before the experiments, the mice were randomly selected for the experimental groups. Swab samples were given blinded to the scientist that performed the analyses.

Patient Samples and Ethics Approval. Wounds of 30 patients with molecularly confirmed autosomal RDEB (OnlineMendelian Inheritance inMan no. 22600) were analyzed for bacterial colonization, as a non-RDEB control group served

http://doc.rero.ch

patients with infected chronic venous ulcers. At the time of sample collection (serum and wound biopsies), all patients (RDEB and non-RDEB) had at least one acutely infected wound, as determined with clinical criteria and a wound swab culture. Healthy volunteers with no ongoing localized or systemic infection served as controls. The study was performed in accordance with the Declaration of Helsinki, approved by the ethics committee of the University of Freiburg (approval no. 45/03). The patients gave written informed consent before their participation.

Mice. RDEB mice and wild-type littermates were on a mixed C57BL/6:129sv background, and tamoxifen-inducible *Col7a1* knockout mice were on C57BL/6 background (3, 38). For deletion of *Col7a1* in tamoxifen-inducible knockout mice, 4-wk-old mice received i.p. 2 μg of tamoxifen dissolved in corn oil on 5 consecutive days. The excision efficiency was analyzed by PCR on DNA from tail biopsies collected after completion of tamoxifen treatment as previously described (38). Control mice received injections with corn oil alone.

The mice were kept in a pathogen-free facility at the University of Freiburg with ad libitum access to food and water; RDEB mice were also provided a soft food diet (1). Mixed male and female mice were used for the analyses. The studies using mice were approved by the regional review board (Regierungspräsidium Freiburg, Freiburg, Germany; approval nos. 35/9185.81/G14-93, 35/9185.81/G09-80, and 35/9185.81/G11-70).

Antibodies. The following cochlin antibodies were used: rat anti-cochlin (clone 9A10D2; BD Biosciences; detecting the cochlin LCCL domain, used for detection of free LCCL domain in serum, analysis of recombinant cochlin domains, and Western blotting), mouse anti-cochlin (Sigma-Aldrich; raised against full-length cochlin and used for detection of free LCCL domain in serum and analysis of recombinant cochlin domains), goat anti-cochlin (Santa Cruz Biotechnology; recognizing the VWFA domains and used for immunofluorescence staining), and rabbit anti-cochlin (Santa Cruz Biotechnology; recognizing the VWFA domains and used for Western blotting and immunofluorescence staining).

The following additional antibodies were used: rabbit anti-collagen VII (Merck Millipore), rabbit anti-collagen VII (40), goat anti-collagen VII (Novus Biologicals), rat anti-VEGFR2 clone Avas 12α1, rat anti-Cd3e (clone 17A2), rat anti-B220 (clone RA3-6B2), rat anti-FDC-M1 (Mfge8), rat anti-integrin β4 (clone 346-11A) (BD Biosciences), rat anti-Cd11b clone M1/70 (BD Biosciences), mouse anti–pan-phospho-tyrosine (PY20) (Abcam), rat anti-metallophilic macrophages antibody (MOMA-1) (ab183549) (Abcam), rat anti-integrin α6 (clone GoH3) (Progen), rabbit anti–β-tubulin, rat anti–ER-TR7, rabbit anti–IL-6, rabbit anti-mouse IL-1β (Abcam), rabbit anti-human collagen I (Acris antibodies), rat anti-mouse C1q (clone 7H8) (Hycult Biotech), mouse anti-αSMA (clone 1A4) (Sigma-Aldrich), rat anti-F4/80 (clone BM8) (eBioscience), rabbit anti-laminin 332, and rat anti-laminin α5, as previously described (1).

Immunofluorescence Microscopy and Western Blotting. For immunofluorescence staining, spleens were removed immediately after killing, embedded in Tissue-Tek CRYO-OCT (Sakura), and snap-frozen. Sections were prepared for immunofluorescence analysis and stained with antibodies as previously described (1). Paraffin sections were digested with 0.05% pronase (Sigma) at 37 °C for 20 min to retrieve antigens. Confocal microscopy was performed with a LSM-I-2 Zeiss LSM 510 microscope equipped with 488-, 541-, 543-, and 633-nm lasers, and images were processed with the Zen 2012 software (Zeiss).

Protein lysates were prepared by pulverizing snap-frozen spleens by using mortar and pestle, followed by either resuspension in Nonidet P-40–containing lysis buffer for immunoprecipitation analysis or by boiling in Laemmli loading buffer containing 8 M urea (3). The samples were analyzed by Western blotting, as previously described (3). ImageJ (NIH) was used for quantification of acquired immunofluorescence images and Western blots.

Proteomic Analysis. Whole-protein lysates from forepaws from six wild-type and six RDEB mice, 4–12 wk of age, were prepared for label-free proteomics and analyzed as previously described (3).

PCR Analysis. RNA was extracted from spleen or splenic stromal cells using NucleoSpin RNA isolation kit (Macherey-Nagel) and reverse transcribed to cDNA with First Strand cDNA Synthesis Kit (Thermo Fisher Scientific). qPCR analysis was performed by a CFX96 Real-Time system (Bio-Rad). The following primers were used: *Col7a1*F, gtttgccacagtgcagtaca; *Col7a1*R, cgtgcgagtgttaccacctt; *Gapdh*F, tcaatgaaggggtcgttgat; *Gapdh*R, cgtcccgtagacaaaatggt; *Coch*F, ttacccctcggaaacctac; *Coch*R, acacgtgggtctcgttcaa; *Cd19*F, ctgggactatccatccacca; *Cd19*R, tgtctccgaggaaacctgac; *Cd3e*F, ctgtctagagggcacgtcaa; *Cd3e*R, gatgcggtggaacactttct; *Cd45*F, tatggttgtgcttggagggt; *Cd45*R, atttgcccttctggacacag; *Acta2*F, gttcagtggtgcctctgtca; *Acta2*R, actgggacgacatggaaaag; *Itga6*F, cctgttctgttcgcccctct; *Itga6*R, ggagcctcttcggcttct; *Itgb4*F, ctfcaactccttccaggtct; I*tgb4*R, atcctggacaatggcaagtc; *Adamts4*F, ggaggaggagatcgtgtttcc; *Adamts4*R, gctgccatcttgtcatctgctac; *Adamts5*F, atcttttcgccatgagcagtg; and *Adamts5*R, ggtactcgccagttttcttcttc.

Cloning and Expression of Cochlin Domains. Mouse *Coch* cDNA was amplified from whole mouse spleen cDNA by PCR using *Coch* forward primer, tactcgaggaccctcgtccaggatccct, and *Coch* reverse primer, atgcggccgcttattgctgggattctaagaagtctc, and subcloned into the pCR4-Topo vector (Invitrogen) following the manufacturer's instruction. The cDNA corresponding to the VWFA 1 and 2 domains, respectively, were subsequently amplified by PCR with the following primers: VWFA 1 forward carrying the Nhe I restriction site, a start codon, and the human interleukin 2 signal peptide, gctagcatgtacaggatgcaactcctgtcttgcattgcactaagtcttgcacttgtcacaaacagtgacattgcatttctatt; VWFA 1 reverse carrying the Xho I restriction site and a FLAG-tag, ctcgagttacttgtcgtcatcgtctttgtagtcgagcttctgcaccagagg; VWFA 2 forward carrying the Nhe I restriction site, a start codon, and the human interleukin 2 signal peptide, gctagcatgtacaggatgcaactcctgtcttgcattgcactaagtcttgcacttgtcacaaacagtaacattgcctttctgattgac; and VWFA 2 reverse carrying the Xho I restriction site and a FLAG-tag, ctcgagttacttgtcgtcatcgtctttgtagtcttgctgggattctaagaagtctct. After digestion with Nhe I and Xho I (Thermo Fisher Scientific), the fragments were inserted into the mammalian expression vector pcDNA3.1+ (Invitrogen) and sequenced by Sanger sequencing. Mouse cochlin LCCL domain corresponded to the sequence catgccctcgtccaggatccctgctctctgcctcggtgcgtggctgctgctgctgctgctgccccggttcgcgcgcgccgagggagcggttcccattcctgtcacctgctttaccagaggcctggatatccgaaaagagaaagcagatgttctctgcccaggaggctgctctcttgaggaattctctgtgtttgggaacatagtgtatgcgtcagtgtccagcatctgcggcgctgctgtccataggggagtgattggcacctcaggggacctgtgcgtgtctacagccttcctggtcgagagaactactcctcggtagatgccaacggcatccagtctcagatgctttcccgatggtccgcgtccttctacccatacgatgttccagattacgcttaa, containing the native signal sequence, and a C-terminal HA tag was synthesized by Genecust.

HEK-293 cells were transfected with the plasmids using Lipofectamine 2000 (Invitrogen). The cells were selected with G418 (Invitrogen) and proteins produced in serum-free medium. After collection, the media were precipitated with 80% saturated ammonium sulfate at +4 °C, the resulting pellet was dissolved in TBS, and the peptides were purified using the HA or FLAG antibody-conjugated Sepharose beads (Thermo Fisher Scientific). The purified peptides were separated by 15% Tricine-SDS/PAGE and analyzed by Coomassie Brilliant Blue staining and Western blotting.

Solid-Phase Binding Assay. Human recombinant cochlin (R&D Systems) and collagen IV (Sigma-Aldrich) were purchased, recombinant human collagen VII was expressed and purified as previously described (48), and recombinant cochlin LCCL and VWFA 1 and 2 domains were purified as described above. One hundred nanograms of cochlin, LCCL domain, VWFA1 domain, and domain 2 diluted in PBS were immobilized on 96-well plates (MaxiSorp microtiter plates; Nunc) and blocked with 0.1% BSA in PBS for 1 h at room temperature (RT). After removal of the blocking buffer, increasing collagen concentrations were added to the wells. After 1-h incubation at RT, the wells were washed with PBS, and HRP-conjugated secondary antibodies were added for 1 h. Subsequently, the wells were washed with PBS, and reactions were developed with *o*-phenylenediamine (Sigma-Aldrich) for 30 min. The plates were read on an ELISA reader at 450 nm, with 695 nm as reference.

Isolation of Splenic Stromal Cells. Freshly isolated spleens were cut into small pieces and digested with 500 U/mL collagenase type I (Worthington) for 1 h at 37 °C. The resulting slurry was then passed through a 70-μm cell strainer, diluted in DMEM:F12 supplemented with 10% FCS (Thermo Fisher Scientific), and seeded in tissue culture flasks (Nunc). One hour after seeding, loose and nonadherent cells were removed by washing three times with PBS. The cells were passaged before analyses and cultured in the presence of 50 μg/mL ascorbic acid (added fresh daily) before assays. The purity of the cell population and absence of hematopoietic cells were analyzed by PCR.

RAW 264.7 Cell Culture and Treatment. RAW 264.7 cells were a kind gift from Dr. Catherine Moali and Agnès Tessier [Institute of Biology and Chemistry of Proteins (IBCP), Lyon, France]. The cells were cultured in DMEM supplemented with 10% FCS. One day before treatment, the cells were serum starved in DMEM with no FCS. The cells were treated for 5 or 30 min with 0.3 μg/mL cochlin LCCL domain, after which they were lysed in Nonidet P-40 lysis buffer. The lysates were analyzed by Western blotting. As control for reactivity, cells were in parallel treated with LPS (Sigma).

http://doc.rero.ch

Analysis of Particle Conducting Ability. Eight-week-old mice received tail vein injections with 100 μL of PBS–10-kDa FITC-dextran (Sigma-Aldrich) solution. After 10 min, spleens were removed and processed for analysis by (immuno) fluorescence imaging as described above.

Injection of Collagen VII and Cochlin LCCL Domain, and Bacterial Sampling. RDEB mice were injected with 20 μg of human recombinant collagen VII in PBS. The mice were injected i.p. close to the spleen, and PBS injections were used as vehicle control. Bacterial swabs of forepaws and snout were collected just before the injection and 1 wk thereafter. Bacteria were cultured either on blood agar or LB agar plates. After killing, blood was collected by heart puncture and 8 μL of sera were analyzed by Western blotting on a 4–18% polyacrylamide gradient gel. Spleen and skin sections were embedded in optimal cutting temperature compound and snap-frozen or fixed in formalin and embedded in paraffin.

For treatment with the LCCL domain, RDEB mice ($n = 6$) were i.p. injected with 30 μg of murine recombinant cochlin LCCL domain in PBS on 2 consecutive days. Bacterial swab samples of forepaws and snout were collected before the injection, and 2 and 5 d after the last injection, and processed as described above. PBS-injected RDEB mice were used as vehicle control.

Statistical Analysis. Shapiro–Wilk normality test was used to test normal distribution. Equal variance was tested for by *F* test. The GraphPad Prism 5.03 software was used for statistical analysis, and data were analyzed using paired, unpaired Student's *t* test, unpaired *t* test with Welch's correction, and Mann–Whitney *U* test as indicated.

ACKNOWLEDGMENTS. We thank Dr. Catherine Moali and Agnès Tessier (IBCP) for providing RAW 264.7 cells. This work was supported by grants from the German Federal Ministry for Education and Research under the frame of Erare-2, the ERA-Net for Research on Rare Diseases (SpliceEB) (to A.N.), and under the frame of Erare-4 (EBThera) (to L.B.-T.); Grants NY90/2-1 and NY90/3-2 (to A.N.), KI1795/1-1 (to D.K.), and BR1475/12-1 (to L.B.-T.) from the German Research Foundation; and Debra International Bruckner-Tuderman 4 (to L.B.-T.) and Nystrom Bruckner-Tuderman 1 (to A.N. and L.B.-T.).

1. Nyström A, et al. (2013) Collagen VII plays a dual role in wound healing. *J Clin Invest* 123:3498–3509.
2. Guerra L, Odorisio T, Zambruno G, Castiglia D (2017) Stromal microenvironment in type VII collagen-deficient skin: The ground for squamous cell carcinoma development. *Matrix Biol* 63:1–10.
3. Nyström A, et al. (2015) Losartan ameliorates dystrophic epidermolysis bullosa and uncovers new disease mechanisms. *EMBO Mol Med* 7:1211–1228.
4. Fine J-D, Johnson LB, Weiner M, Li K-P, Suchindran C (2009) Epidermolysis bullosa and the risk of life-threatening cancers: The National EB Registry experience, 1986-2006. *J Am Acad Dermatol* 60:203–211.
5. Mittapalli VR, et al. (2016) Injury-driven stiffening of the dermis expedites skin carcinoma progression. *Cancer Res* 76:940–951.
6. Naba A, et al. (2016) The extracellular matrix: Tools and insights for the "omics" era. *Matrix Biol* 49:10–24.
7. van der Kooi-Pol MM, et al. (2013) High anti-staphylococcal antibody titers in patients with epidermolysis bullosa relate to long-term colonization with alternating types of *Staphylococcus aureus*. *J Invest Dermatol* 133:847–850.
8. Hoste E, et al. (2015) Innate sensing of microbial products promotes wound-induced skin cancer. *Nat Commun* 6:5932.
9. Kaneko K, et al. (2000) Renal amyloidosis in recessive dystrophic epidermolysis bullosa. *Dermatology* 200:209–212.
10. Pfendner EG, Lucky AW (1993) Dystrophic epidermolysis bullosa. *GeneReviews*, eds Pagon RA, et al. (University of Washington, Seattle). Available at https://www.ncbi.nlm.nih.gov/books/NBK1304/. Accessed March 6, 2017.
11. Vindenes H, Bjerknes R (1995) Microbial colonization of large wounds. *Burns* 21:575–579.
12. Bajénoff M, et al. (2006) Stromal cell networks regulate lymphocyte entry, migration, and territoriality in lymph nodes. *Immunity* 25:989–1001.
13. Gretz JE, Norbury CC, Anderson AO, Proudfoot AE, Shaw S (2000) Lymph-borne chemokines and other low molecular weight molecules reach high endothelial venules via specialized conduits while a functional barrier limits access to the lymphocyte microenvironments in lymph node cortex. *J Exp Med* 192:1425–1440.
14. Roozendaal R, et al. (2009) Conduits mediate transport of low-molecular-weight antigen to lymph node follicles. *Immunity* 30:264–276.
15. Song J, et al. (2013) Extracellular matrix of secondary lymphoid organs impacts on B-cell fate and survival. *Proc Natl Acad Sci USA* 110:E2915–E2924.
16. Py BF, et al. (2013) Cochlin produced by follicular dendritic cells promotes antibacterial innate immunity. *Immunity* 38:1063–1072.
17. Robertson NG, et al. (1998) Mutations in a novel cochlear gene cause DFNA9, a human nonsyndromic deafness with vestibular dysfunction. *Nat Genet* 20:299–303.
18. Goel M, et al. (2012) Cochlin, intraocular pressure regulation and mechanosensing. *PLoS One* 7:e34309.
19. Jung J, Kim HS, Lee MG, Yang EJ, Choi JY (2015) Novel COCH p.V123E mutation, causative of DFNA9 sensorineural hearing loss and vestibular disorder, shows impaired cochlin post-translational cleavage and secretion. *Hum Mutat* 36:1168–1175.
20. Lokmic Z, et al. (2008) The extracellular matrix of the spleen as a potential organizer of immune cell compartments. *Semin Immunol* 20:4–13.
21. Mueller SN, Germain RN (2009) Stromal cell contributions to the homeostasis and functionality of the immune system. *Nat Rev Immunol* 9:618–629.
22. Bajénoff M, Germain RN (2009) B-cell follicle development remodels the conduit system and allows soluble antigen delivery to follicular dendritic cells. *Blood* 114:4989–4997.
23. South AP, Uitto J (2016) Type VII collagen replacement therapy in recessive dystrophic epidermolysis bullosa—how much, how often? *J Invest Dermatol* 136:1079–1081.
24. Zhang LJ, et al. (2015) Innate immunity. Dermal adipocytes protect against invasive *Staphylococcus aureus* skin infection. *Science* 347:67–71.
25. Fritsch A, et al. (2008) A hypomorphic mouse model of dystrophic epidermolysis bullosa reveals mechanisms of disease and response to fibroblast therapy. *J Clin Invest* 118:1669–1679.
26. Jaspars LH, De Melker AA, Bonnet P, Sonnenberg A, Meijer CJ (1996) Distribution of laminin variants and their integrin receptors in human secondary lymphoid tissue. Colocalization suggests that the alpha 6 beta 4-integrin is a receptor for laminin-5 in lymphoid follicles. *Cell Adhes Commun* 4:269–279.
27. Ogata T, Yamakawa M, Imai Y, Takahashi T (1996) Follicular dendritic cells adhere to fibronectin and laminin fibers via their respective receptors. *Blood* 88:2995–3003.
28. Zutter MM (1991) Immunolocalization of integrin receptors in normal lymphoid tissues. *Blood* 77:2231–2236.
29. van den Berg TK, van der Ende M, Döpp EA, Kraal G, Dijkstra CD (1993) Localization of beta 1 integrins and their extracellular ligands in human lymphoid tissues. *Am J Pathol* 143:1098–1110.
30. Kranich J, et al. (2008) Follicular dendritic cells control engulfment of apoptotic bodies by secreting Mfge8. *J Exp Med* 205:1293–1302.
31. Schwaeble W, et al. (1995) Follicular dendritic cells, interdigitating cells, and cells of the monocyte-macrophage lineage are the C1q-producing sources in the spleen. Identification of specific cell types by in situ hybridization and immunohistochemical analysis. *J Immunol* 155:4971–4978.
32. Tampoia M, et al. (2013) Prevalence of specific anti-skin autoantibodies in a cohort of patients with inherited epidermolysis bullosa. *Orphanet J Rare Dis* 8:132.
33. Woodley DT, et al. (2014) De novo anti-type VII collagen antibodies in patients with recessive dystrophic epidermolysis bullosa. *J Invest Dermatol* 134:1138–1140.
34. Has C, Nyström A (2015) Epidermal basement membrane in health and disease. *Curr Top Membr* 76:117–170.
35. Nagy I, Trexler M, Patthy L (2008) The second von Willebrand type A domain of cochlin has high affinity for type I, type II and type IV collagens. *FEBS Lett* 582:4003–4007.
36. Vondenhoff MFR, et al. (2008) Separation of splenic red and white pulp occurs before birth in a LTalphabeta-independent manner. *J Leukoc Biol* 84:152–161.
37. Dijkstra CD, Döpp EA (1983) Ontogenetic development of T- and B-lymphocytes and non-lymphoid cells in the white pulp of the rat spleen. *Cell Tissue Res* 229:351–363.
38. Kühl T, et al. (2016) Collagen VII half-life at the dermal-epidermal junction zone: Implications for mechanisms and therapy of genodermatoses. *J Invest Dermatol* 136:1116–1123.
39. Woodley DT, et al. (2013) Intravenously injected recombinant human type VII collagen homes to skin wounds and restores skin integrity of dystrophic epidermolysis bullosa. *J Invest Dermatol* 133:1910–1913.
40. Kühl T, et al. (2015) High local concentrations of intradermal MSCs restore skin integrity and facilitate wound healing in dystrophic epidermolysis bullosa. *Mol Ther* 23:1368–1379.
41. Umemoto H, et al. (2012) Type VII collagen deficiency causes defective tooth enamel formation due to poor differentiation of ameloblasts. *Am J Pathol* 181:1659–1671.
42. Bateman JF, Boot-Handford RP, Lamandé SR (2009) Genetic diseases of connective tissues: Cellular and extracellular effects of ECM mutations. *Nat Rev Genet* 10:173–183.
43. Carmignac V, et al. (2011) Autophagy is increased in laminin α2 chain-deficient muscle and its inhibition improves muscle morphology in a mouse model of MDC1A. *Hum Mol Genet* 20:4891–4902.
44. Grafe I, et al. (2014) Excessive transforming growth factor-β signaling is a common mechanism in osteogenesis imperfecta. *Nat Med* 20:670–675.
45. Grumati P, et al. (2010) Autophagy is defective in collagen VI muscular dystrophies, and its reactivation rescues myofiber degeneration. *Nat Med* 16:1313–1320.
46. Neptune ER, et al. (2003) Dysregulation of TGF-beta activation contributes to pathogenesis in Marfan syndrome. *Nat Genet* 33:407–411.
47. van der Kooi-Pol MM, et al. (2012) High genetic diversity of *Staphylococcus aureus* strains colonizing patients with epidermolysis bullosa. *Exp Dermatol* 21:463–466.
48. Bornert O, et al. (2016) Analysis of the functional consequences of targeted exon deletion in COL7A1 reveals prospects for dystrophic epidermolysis bullosa therapy. *Mol Ther* 24:1302–1311.

http://doc.rero.ch